Robust Graphene Membranes in a Silicon Carbide Frame

Daniel Waldmann,[†] Benjamin Butz,[‡] Sebastian Bauer,[§] Jan M. Englert,[⊥] Johannes Jobst,[†] Konrad Ullmann,[†] Felix Fromm,[∥] Maximilian Ammon,[#] Michael Enzelberger,[#] Andreas Hirsch,[▽] Sabine Maier,[#] Patrik Schmuki,[§] Thomas Seyller,[⊗] Erdmann Spiecker,[‡] and Heiko B. Weber[†,*]

[†]Lehrstuhl für Angewandte Physik, [‡]Center for Nanoanalysis and Electron Microscopy, [§]Lehrstuhl für Korrosion und Oberflächentechnik, [⊥]Institute of Advanced Materials and Processes, [∥]Lehrstuhl für Technische Physik, [#]Lehrstuhl für Experimentalphysik, [▽]Lehrstuhl für Organische Chemie II, Universität Erlangen-Nürnberg, Germany and [⊗]Institut für Physik, Technische Universität Chemnitz, Germany

ABSTRACT We present a fabrication process for freely suspended membranes consisting of bi- and trilayer graphene grown on silicon carbide. The procedure, involving photoelectrochemical etching, enables the simultaneous fabrication of hundreds of arbitrarily shaped membranes with an area up to 500 μm^2 and a yield of around 90%. Micro-Raman and atomic force microscopy measurements confirm that the graphene layer withstands the electrochemical etching and show that the membranes are virtually unstrained. The process delivers membranes with a cleanliness suited for high-resolution transmission electron microscopy (HRTEM) at atomic scale. The membrane, and its frame, is very robust with respect to thermal cycling above 1000 °C as well as harsh acidic or alkaline treatment.

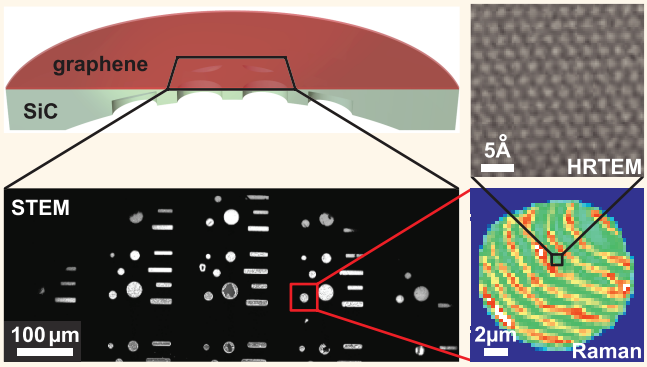

KEYWORDS: epitaxial graphene · membranes · photo-assisted etching · Raman spectroscopy · transmission electron microscopy

Graphene is a unique two-dimensional material. Although it is atomically thin, it has an enormous material strength.[1] Therefore, graphene membranes are considered as important new tool, for example, as support for transmission electron microscopy, as ultimately thin and impermeable membranes,[2] or for DNA sequencing.[3] Furthermore, membranes are an ideal configuration to study the microstructure and morphology of graphene by transmission electron microscopy (TEM). We focus on graphene grown by thermal decomposition of silicon carbide. This material is available in high quality on large areas[4,5] and has extensively been investigated with regard to electronic applications.[5−8] With respect to membranes, which have not been reported so far for graphene grown on SiC, this material system has the advantage of being robust and chemically inert. Moreover, the graphene layer is tightly connected (with epitaxial control) to the SiC substrate frame.

The structure of graphene membranes renders it a perfect candidate for TEM investigations, which, in turn, have been carried out on material obtained from mechanical exfoliation,[9] chemical vapor deposition on metal surfaces,[10] or chemical exfoliation.[11,12] In particular, high-resolution TEM (HRTEM) is used to study defects, grain boundaries, or the incorporation of dopands into the graphene sheet.[13−16] These fabrication methods, however, necessitate a transfer of graphene to suited TEM grids,[12,17,18] which can be avoided with the approach presented here. For graphene grown on SiC, on the other hand, HRTEM is so far only conducted in cross section[19] as membranes were not available. In this letter, we present a reliable, high-yield fabrication method for freely spanned membranes consisting of bi- and trilayer graphene. This development enables detailed plan-view TEM characterization and provides a platform for new types of experiments.

RESULTS AND DISCUSSION

Fabrication. The fabrication process is based on the photoelectrochemical removal of the

* Address correspondence to heiko.weber@physik.uni-erlangen.de.

Received for review March 1, 2013 and accepted April 15, 2013.

Published online April 15, 2013
10.1021/nn401037c

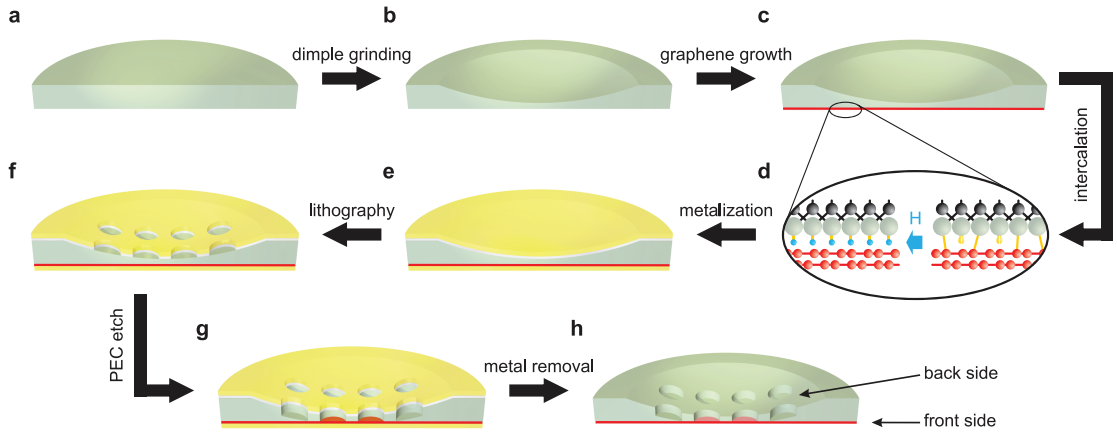

Figure 1. Scheme of the fabrication process. (a) Starting point is a disc of 3 mm diameter of n-type SiC, which is thinned to ≈100 μm by mechanical polishing. (b) The sample is dimple ground to a final thickness of 2−10 μm in its center. (c) Graphene is grown in argon atmosphere following the process developed by Emtsev *et al.*[4] (d) If quasi-freestanding graphene is desired, hydrogen intercalation is performed using the procedure described in ref 20. (e) A gold layer is evaporated on the front side and a titanium/gold layer on the back side of the sample. (f) The etching mask is patterned using e-beam lithography and wet chemistry. (g) The SiC substrate is selectively removed using photoelectrochemical (PEC) etching. (h) Protective and etching mask are removed by wet chemistry and the sample is critical-point dried.

SiC underneath the graphene layers such that the membrane spans over a hole through the entire substrate. A sketch of the manufacturing process is shown in Figure 1. The n-type SiC substrate is ultrasonically cut into discs of 3 mm diameter, thus, fitting into standard TEM holders. Moreover, it is thinned down to a few micrometers in the center of the disc using dimple grinding from the back side. Subsequently, the graphene layers are grown in argon atmosphere on the front side (SiC(0001) basal plane) of the chip following the process developed by Emtsev *et al.*[4] The growth temperature of 1750 °C is chosen such that around 60% of the sample area is covered with monolayer graphene and 40% with bilayer graphene. This ensures that no areas without graphene remain. The graphene layers reside on a $(6\sqrt{3} \times 6\sqrt{3})R30°$ reconstruction layer that is partially covalently bound to the SiC substrate and is often referred to as buffer layer.[21] As-prepared graphene is called MLG (monolayer graphene) in the following. For some of the samples presented here, the buffer layer is converted to a graphene layer by the intercalation of hydrogen,[22] resulting in bilayer graphene. This material is termed quasi-freestanding bilayer graphene (QFBLG) as the hydrogen intercalation reduces the interaction between the graphene layers and the SiC substrate.[20] Despite remarkable differences in the electronic properties of MLG and QFBLG on SiC substrate, both materials show very similar results concerning the presented structural characterization after the substrate is removed. Hence, in the following, the distinction between the two graphene materials is only explicitly made where it is necessary for the interpretation of the findings.

Immediately after growth, the graphene is covered with a 40 nm gold layer to keep it free from contamination during the following process steps and to protect the graphene layer from the harsh environment during the electrochemical etching. If no protective layer is used on top of graphene, it is heavily damaged during the etching process. A titanium/gold etching mask is defined on the back side of the sample by standard e-beam lithography: Titanium and gold are evaporated on the back side of the sample and a lithographically structured PMMA resist serves as mask for the subsequent wet-chemical removal of the metals. The gold is dissolved in an iodine/potassium iodine solution and the titanium is removed in 1% hydrofluoric acid. In this way, the back side of the sample can be densely covered with arbitrarily shaped structures that predefine shape and position of the suspended membranes. Wherever the titanium/gold mask is removed, graphene layers, which are occasionally grown on the back side of the sample, are removed by reactive ion etching in oxygen plasma. Subsequently, the SiC substrate is exposed to the electrochemical etching process in these unprotected areas.

SiC is known as an extremely robust material that withstands harsh acidic and alkaline conditions. It can, however, be electrochemically etched in potassium hydroxide solution when hole-type charge carriers are present[23] following the reaction:

$$SiC + 8OH^- + 6h^+ \rightarrow [Si(OH)_2O_2]^{2-} + CO + 3H_2O \quad (1)$$

For n-type SiC, the holes h^+ can be provided by applying ultraviolet light. For this purpose, we use a HeCd laser with a wavelength of 325 nm. A similar setup was used by Shivaraman *et al.* to underetch nanomechanical resonators of graphene grown on SiC.[24] An etching rate of 4 μm/h is obtained by applying the maximal laser intensity, but a smaller rate can

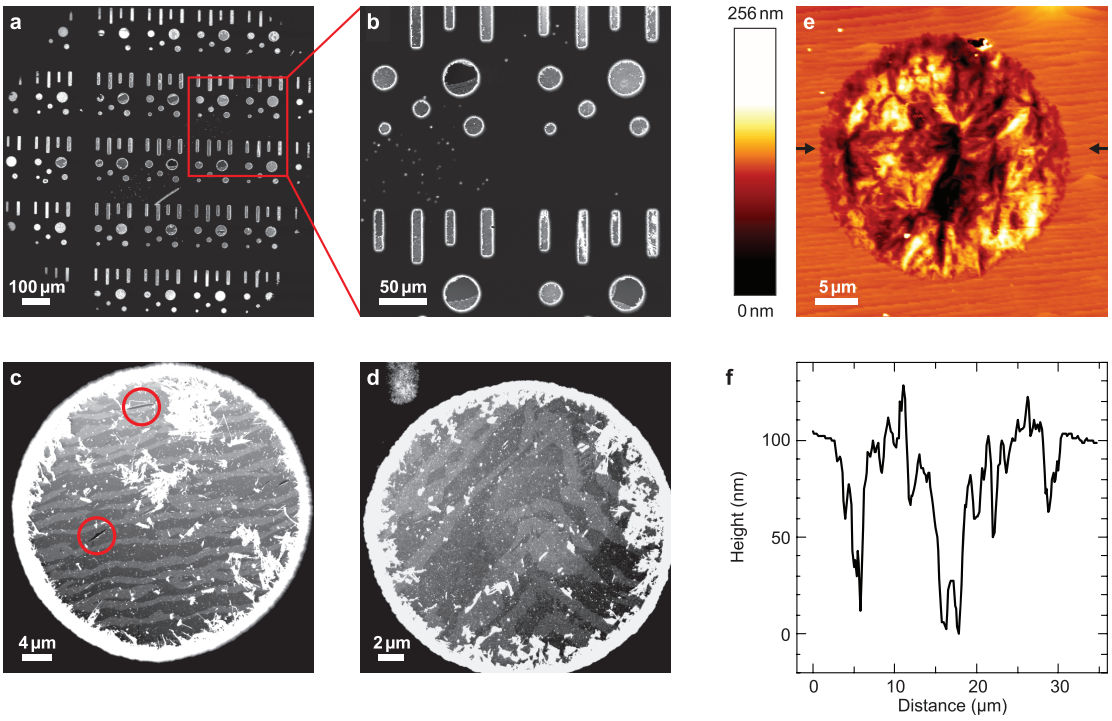

Figure 2. (a) Dark field (DF) scanning transmission electron microscopy (STEM) image obtained at 10 kV of >200 membranes processed in parallel on one sample. A yield of approximately 90% is achieved. Only for the largest circular membranes (diameter 25 μm), the yield is reduced to ≈30%. (b) Detailed view of panel a. (c and d) DF-STEM image of membranes with a diameter of 25 and 15 μm, respectively. Red circles in panel c indicate small cracks in the membrane. (e) Atomic force microscopy measurement of a membrane with 25 μm diameter, obtained in tapping mode (free oscillation amplitude 200 nm, force constant 9 N/m). (f) Corresponding section taken at the line indicated by arrows in panel e.

be adjusted by reducing the UV light intensity. Note that no large-angle etch pits are formed but rather vertical-wall, projective etching takes place due to the shadows cast by the protective metal layer. As a result of the increasing sample thickness in radial direction, the membranes in the center become freestanding first, and suspended membranes are created more distant from the center subsequently. A duration of the etching that leads to an etching depth of three times of the minimal sample thickness is typically used. This implies etching times of 2−6 h and leads to suspended membranes in a circle around the center of the sample with a diameter of a few hundred micrometers (see Figure 2a). Thus, hundreds of arbitrarily shaped membranes can be fabricated simultaneously. After etching, the gold layer on top of the graphene and the gold/titanium etching mask are removed in an iodine/potassium iodine solution and 1% hydrofluoric acid. Using X-ray photoelectron spectroscopy, we confirmed that the gold is entirely removed. To prevent rupture of the membranes when taking the sample out of the liquid, a critical point drying system is used.

For all fabricated rectangular membranes (widths up to 7 μm and lengths up to 40 μm) and circular membranes with diameters up to 20 μm, a yield of around 90% is achieved. Larger circular membranes tend to rupture and for membranes with a diameter of 25 μm the yield is reduces to ≈30%. In Figure 2b, three ruptured and one intact membrane with a diameter of 25 μm are shown among many intact smaller membranes. Small cracks are often observed in the largest circular membranes but rarely in the smaller ones (see Figure 2c,d). A closer look at the membranes at the rim of the area in Figure 2 reveals that just before the membranes become free-standing, pieces of SiC residuals with irregular, sometimes dendritic shape are present. They appear bright in dark-field scanning transmission electron microscopy (DF-STEM). On membranes closer to the sample center, rod-like residuals are occasionally found in various concentrations. Using energy dispersive X-ray spectroscopy (EDX), we confirmed that these residuals consist of SiC that is probably redeposited when the etching process is stopped. This agrees well with AFM measurements on top of the membranes (Figure 2e), where such rod-like residuals were not observed implying that they are adsorbed on the etched side of the membrane. However, most of the membrane area is free from these contaminations (see Figure 2c,d). In particular, no contaminations from the chemicals involved in the fabrication process are found with EDX on the whole membrane except a very small amount of fluorine. The stripe-like features seen in Figure 2c−e are caused by the contrast variations between two to three carbon layers. This arrangement of areas with different graphene layer count is a well-known

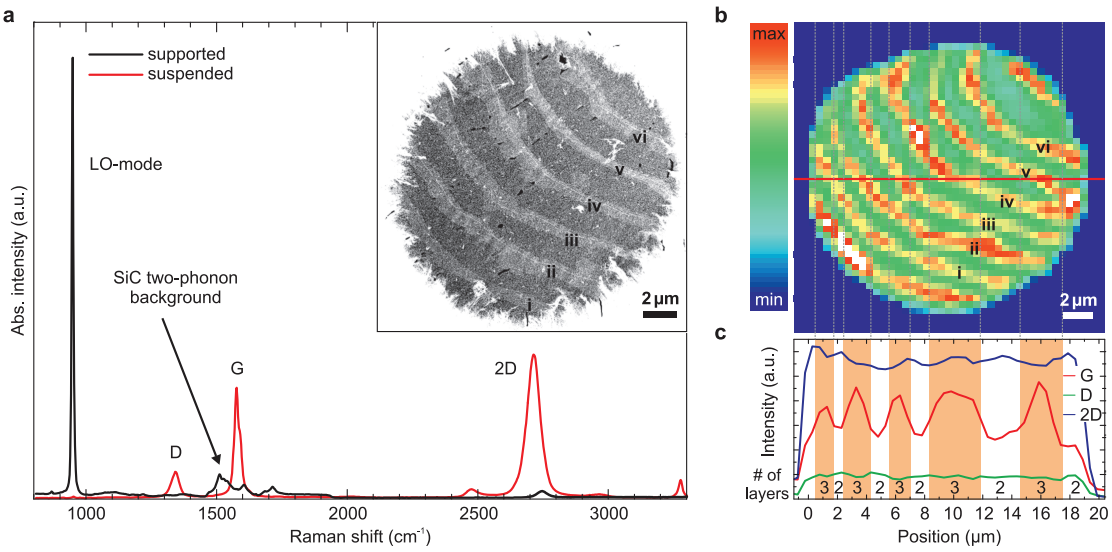

Figure 3. (a) Confocal Raman spectra of bilayer regions in a MLG sample. The `suspended' spectrum is recorded from a freestanding membrane, while the `supported' spectrum was collected outside the membrane but within the same measurement and hence, with identical parameters. The distinction is made from the LO phonon mode of SiC and the residual two-phonon background between 1500 and 1900 cm^{-1}. Inset: Secondary electron scanning electron microscopy (SEM) image at 10 kV of a membrane with a diameter of 15 μm. (b) Spatial G-band intensity map of a freely suspended MLG membrane, which is supported by a SiC frame (outer blue area). The stripe-like contrast inside the membrane stems from stepwise variations between two and three graphene layers. The labeling of the stripes matches the labeling of the very same sample in panel a. (c) Raman intensity profile along the horizontal red line in panel b for the three major spectral contributions, namely, G-, D- and 2D-band. The graphene layer count is indicated in the appropriate areas. The low intensity at the outmost data points of the profile indicates the supported region.

feature of graphene growth on SiC.[4] For QFBLG membranes this means that bi- and trilayer graphene areas are present. For membranes made from MLG, however, the question arises whether the buffer layer is converted to a graphene layer by the removal of the substrate. The results of the Raman measurements indicate that the buffer layer is, indeed, converted (see below).

By the proposed fabrication, we expected to obtain monolayer graphene membranes from a QFMLG sample. Unfortunately, such membranes could not yet be prepared. All membranes made from QFMLG were found to be completely destroyed when imaged in STEM after the fabrication process. Although the reason for damaging of the QFMLG membranes is up to now not fully understood, the tensile strain observed in QFMLG[20] might lead to rupture of the membranes when the substrate is removed. In contrast, MLG and QFBLG are compressively strained, and the strain can be released out-of-plane when the substrate is removed.

Raman Characterization. The presented membranes open the possibility to conduct Raman spectroscopy on graphene grown on SiC without the disturbing influence of the substrate (*cf.* Figure 3a). The Raman spectrum of graphene is dominated by three signals denoted as G-, D- and 2D-band in the following. The G-band at a Raman shift of ≈1580 cm^{-1} originates from the zone centered optical phonon. Its full width at half-maximum (fwhm) and position can be used to estimate doping and strain in the sample. As the D-band (located at ≈1350 cm^{-1}) requires a defect for activation, its intensity can be used as a measure for the defect density.[25,26] Its overtone, the 2D band (located at ≈2700 cm^{-1}), however, is not defect related. As it is strongly dependent on the local electronic band structure and mechanical properties it is widely used to determine the number of graphene layers, stress and doping level.[27]

To obtain spatially resolved Raman data, scanning Raman microscopy (SRM) with 532 nm laser excitation was used in a confocal backscattering setup with a 100×/NA = 0.9 objective to reduce background and to allow for submicrometer lateral resolution and high surface sensitivity. By suspending the graphene membranes, we were able to suppress the two phonon SiC signal in the spectral range of the D- and G-bands of graphene to a level that permits the evaluation of the G- and D-band without the need of subtracting a SiC reference spectrum as it is commonly applied[28] (*cf.* Figure 3a). To keep the acquisition times within reasonable limits, whole membranes are typically imaged with a 600 grooves/mm grating (see Figure 3b and Figure 4a), resulting in a spectral resolution of 2.6 cm^{-1} and a resolution power of $R \approx 6500$ in the center of the grating. As this limits the significance of peak positions measured in this mode, high resolution measurements, conducted on a 1800 grooves/mm grating (spectral resolution of 0.7 cm^{-1}, $R \approx 24\,000$), are used when positions are to be discussed.

A striking observation is the significant enhancement of the Raman intensity on the membranes compared to

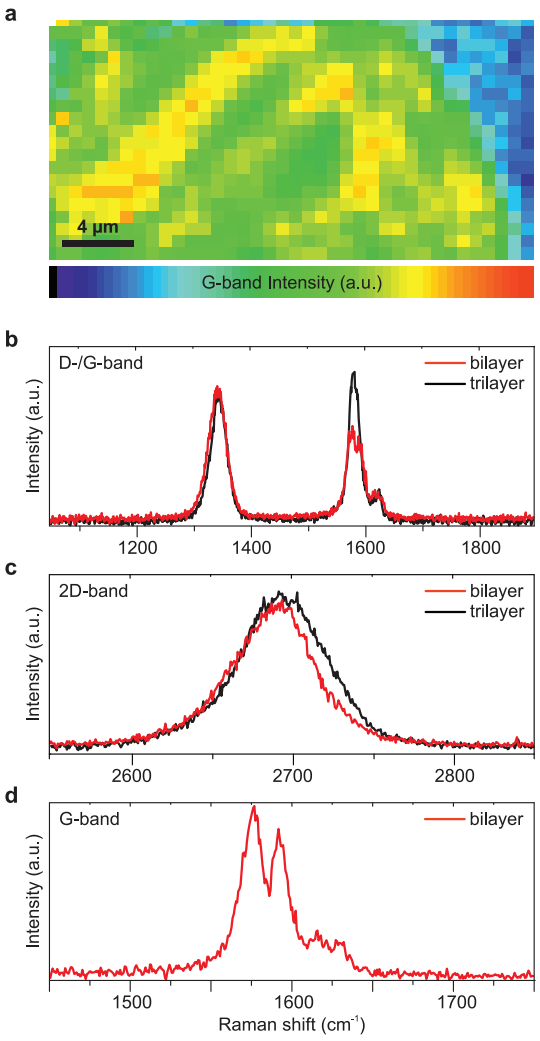

Figure 4. (a) Raman spatial intensity maps for the G-band of a QFBLG membrane. (b and c) Single spectra extracted from areas identified as bi- or trilayer regions by G-band contrast for the D/G-band area or the 2D-band area, respectively. (d) Zoom into the G-band signal of a bilayer area revealing the splitting of the G-band feature.

graphene on SiC substrate. The signal recorded on the membranes fabricated from QFBLG is increased by a factor of approximately five in peak intensity compared to the Raman signal of graphene on SiC as judged from the G-band intensity. This enhancement is also visible for membranes produced from MLG where however, a precise quantification was not possible due to the residual SiC two phonon signal in the supported areas (*cf.* Figure 3a). We thus conclude that the damping of the Raman signal of graphene on SiC, which we observed in several previous measurements, is caused by interactions with the substrate.

Figure 3b shows a G-band intensity map of a membrane fabricated from MLG. The G-band intensity can be assumed to be directly proportional to the number of graphene layers probed by the laser. Hence, it is possible to distinguish areas with different graphene film thicknesses in a G-band intensity map. Theoretically, an increase of the G-band intensity by a factor of 2 is expected when comparing mono- and bilayer graphene, whereas a factor of 1.5 is predicted for a bilayer/trilayer contrast. We observe stripes in the G-band maps (*cf.* Figure 3b), which are caused by the stepwise variations of the number of graphene layers. The stripes continue seamlessly along the whole wafer, undisturbed by the removal of the substrate. Obviously, the stripes correspond to the contrast variations observed in the inset in Figure 3a and are located at the step edges of the SiC substrate. As the G-band intensity varies by a factor of 1.5 in the striped region for membranes fabricated from MLG as well as QFBLG, we conclude that for both membrane types bi- and trilayer areas are present. This is confirmed in the Raman intensity profiles in Figure 3c and gives convincing evidence that the buffer layer of MLG samples is converted to a graphene layer by the removal of the substrate.

Furthermore, the ratio of the D-band intensity over the G-band intensity (I_D/I_G) can be used to estimate the mean distance of defects in graphene.[25] For membranes prepared from MLG, we find rather small values of $I_D/I_G \approx 0.25$ for bilayer areas and $I_D/I_G \approx 0.1$ for trilayer areas (Figure 3a,c). Thus, we conclude that the graphene is well protected from the harsh SiC etching process by the gold protection layer. Outside the membranes, we did not record any noticeable D-band intensity (Figure 3a). Samples that have been intercalated with hydrogen before the metalization show a significantly larger D-band intensity in- and outside the suspended area and exhibit I_D/I_G values of 0.9 in trilayer regions and 1.4 in bilayer regions (see Figure 4b). Furthermore in both samples, QFBLG as well as MLG, the absolute D-band intensity does not change significantly from bi- to trilayers which suggests that the additional graphene layer is essentially defect free (see Figure 3c and Figure 4b). This supports the picture that the defects are concentrated in the lowest graphene layer, which originates from the buffer layer and is affected strongest by hydrogen intercalation and electrochemical etching. The fact that the D- to G-band intensity ratio inside and outside the freestanding membranes does not change for membranes fabricated from QFBLG underlines that the etching procedure does not have a strong influence on the defect concentration of the membranes.

To analyze line widths and peak positions we conducted a high spectral accuracy mapping of a membrane fabricated from QFBLG (*cf.* Figure 4a). According to theory, Bernal stacked bi- and trilayer systems should exhibit a pronounced asymmetry in their respective 2D bands.[27] However, this asymmetry is suppressed in bilayer graphene grown on SiC and manifests only in a slight but almost symmetrical broadening in the 2D-band feature[28,29] (*cf.* Figure 4c). When removing the substrate, the asymmetry is not restored.

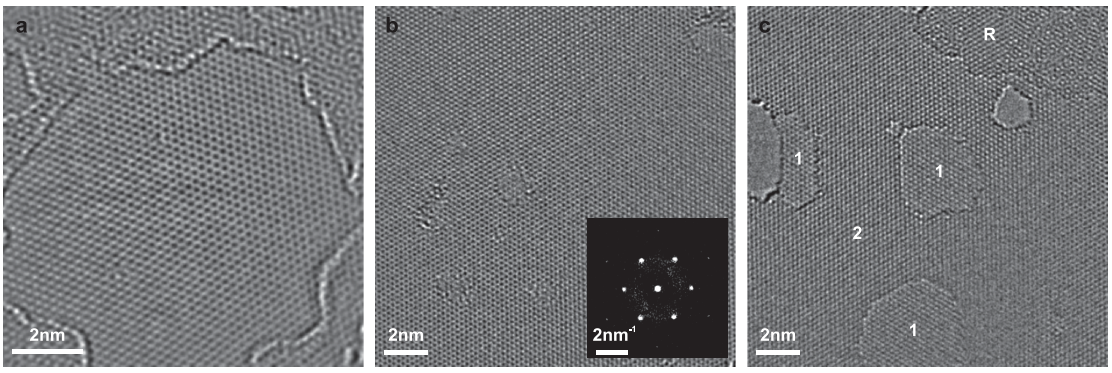

Figure 5. HRTEM images ($|C_s|$ < 5 μm, Fourier-filtered applying bandpass filter 0.5 Å to 1 nm) of suspended graphene membranes. (a) Pristine graphene membrane (bilayer region) before any additional thermal treatment (cleaning). The outer regions show amorphous residuals from the preparation. (b) After thermal treatment at 1070 °C, nearly undamaged regions of bilayer graphene membrane clearly reveal the $\{1\bar{1}00\}$ lattice spacing (inset shows calculated Fourier transform). (c) Nanometer-sized holes were intentionally created by intense electron-beam irradiation in a neighboring region to (b) in order to visualize the local number of graphene layers (1 = monolayer graphene, 2 = bilayer graphene). Graphenoid residuals (R) formed during high-temperature treatment are indicated by a rotational Moiré-pattern in the upper right corner.

We therefore conclude that the absence of the asymmetric peak shape is an intrinsic property of graphene grown on SiC and is not introduced by interactions with the substrate.

The 2D-band position is found at ≈2710 cm^{-1} outside the membrane, indicating that the QFBLG layer is compressively strained in accordance to literature.[30] As the graphene layers relax as a consequence of the removal of the substrate, the 2D-band position is redshifted to values around 2689 cm^{-1} on the membranes. This coincides perfectly with results found for (unstrained) exfoliated bilayer graphene.[31] The release of compressive stress is furthermore explicitly revealed in the AFM images (Figure 2e,f) from the rough topography on the membrane. We find a corrugation of up to 160 nm on the membrane, whereas the atomically smooth surface outside the membrane shows steps of the SiC substrate. By applying surface triangulation methods to the AFM topography image we estimate an average 0.9% linear expansion of the membrane compared to a flat layer. The expansion and corresponding buckling of the membrane appears to be largely isotropic (Figure 2e) indicating relaxation of biaxial compressive stress upon removal of the SiC substrate. In fact, the measured linear expansion nicely corresponds to the relaxation of maximal strain (0.8%) introduced into graphene on 6H-SiC upon cooling from growth temperature as result of the different thermal expansion coefficients.[32]

Since the graphene membrane is relaxed, the G-band position can directly be used to determine the doping level. As the G-band positions at ≈1582 cm^{-1} found on trilayer areas correspond well to values observed for quasi-neutral graphene layers,[33−35] we conclude that the intrinsic doping observed for graphene on SiC is drastically reduced by the removal of the substrate. In the bilayer areas, however, the G-band exhibits a clear splitting with its components centered around 1576 and 1592 cm^{-1} (see Figure 4d). G-band splitting is reported in literature for various situations like asymmetrically doped bilayer graphene,[36] uniaxially strained graphene[37] or due to the occurrence of the R′-peak due to rotated layers.[38] However, presumably none of the above-mentioned scenarios are valid for the G-band splitting of the membranes and its origin remains a topic of further research.

Transmission Electron Microscopy. To analyze the structural properties of the graphene membranes, HRTEM is conducted using an image-side aberration-corrected Titan^3 80−300 microscope. It is operated at 80 kV to prevent knock-on damage of the graphene membranes.[39] Already on the as-prepared membranes (directly after the process sketched in Figure 1, without any further cleaning), 50% of the area is residual-free. This cleanliness is demonstrated in Figure 5a, which depicts a HRTEM micrograph of a representative area of a bilayer region of a membrane prior to any additional heat treatment in the microscope. The amount of residuals can, however, be drastically reduced by heating the sample to temperatures of a few hundred °C or even higher. Furthermore, the membranes withstand *in situ* heating (GATAN double-tilt heating holder) up to temperatures above 1000 °C in the microscope under high-vacuum conditions as Figure 5b,c shows. A nearly undamaged region of a membrane after the thermal treatment is depicted in Figure 5b, whereas Figure 5c shows a neighboring area where tiny holes are intentionally generated by intense electron-beam irradiation in order to visualize the two layers of graphene in this region (the local number of graphene layers is indicated). During the high-temperature treatment, we occasionally observe that carbon-rich residuals locally form small graphenoid crystallites on the graphene membrane. This generates the rotational Moiré pattern, which is visible in Figure 5c (upper right corner, marked with R).

CONCLUSIONS

In conclusion, we present a reliable fabrication technique for bilayer graphene membranes, created from graphene grown on SiC. The membranes are spanned over holes in the SiC substrate frame and can be patterned in various geometries and sizes. The stable and well-defined attachment of the graphene sheet to the substrate is given by its epitaxial growth. These membranes allow for a refined characterization of the graphene layer, for example, Raman studies without the disturbing influence of the substrate and enable TEM studies in plan-view. Furthermore, this chemically and thermally robust membrane system may be a valuable tool for novel experiments.

METHODS

Mechanical Preparation. To facilitate the preparation of membranes from the epitaxial graphene, the SiC was mechanically prepared as follows. First, TEM-conform discs (diameter 3 mm, thickness ~100 μm) were prepared from the original SiC wafers by ultrasonic disc cutting (GATAN Ultrasonic disc cutter, Model No. 601). Second, the discs were thinned down to around 100 μm from the back side. The low rate for KOH etching necessitates further back-thinning of the substrate down to a few micrometer in the region where the membranes form (central region of each TEM sample). Therefore, each sample was dimple ground and polished (GATAN dimple grinder, Model No. 656). This leads to a strongly reduced aspect ratio of the etch channels and thus to a more defined etching behavior.

Photoelectrochemical Etching. We use a HeCd laser (Kimmon IK 3552R-G) with a wavelength of 325 nm and a continuous-wave power of 55 mW (spot diameter ≈2 mm) to provide UV-light for the photoelectrochemical reaction. The electrochemical etching is performed in a 1 wt % potassium hydroxide solution using a standard electrochemical cell, equipped with a platinum counter electrode and a silver/silver chloride reference electrode. The etching is conducted at an anodic potential of 400 mV using a Jaissle 1030DA potentiostat.

Raman Spectroscopy. Scanning Raman microscopy and point spectroscopy was carried out on a Horiba LabRAM Aramis confocal Raman microscope (excitation wavelength 532 nm (2.33 eV)) with diffraction limited laser spot sizes well below 1 μm (Olympus ×100 objective, N.A. 0.90). The incident laser power was kept as low as possible to avoid structural damage to the sample. Specimens were aligned on an optical table and relocated by means of bright field optical microscopy. High resolution single point spectra were obtained with 1800 grooves/mm high precision (0.7 cm^{-1}) optical gratings. Scanning Raman Microscopy was carried out utilizing SWIFT module and with reduced spectral resolution on (600 grooves/mm grating providing 2.6 cm^{-1} resolution at fixed position) in order to keep integration times as low as possible. Focus position was optimized before mapping acquisition by a sequence of confocal depth scans and then fixed to optimized position. Sample light collection was carried out by a multichannel CCD camera and separated from elastically scattered fractions by a holographic notch filter. XY-scanning was conducted by a directly software controlled Mertzhäuser scanning table.

Electron Microscopy. Scanning electron microscopy (SEM) in transmission mode (DF low-kV STEM) was conducted at 10 kV acceleration voltage using a high-resolution Zeiss Supra 40 with Gemini column.

For HRTEM imaging, an image-side aberration-corrected Titan^3 80−300 microscope was used. It was operated at 80 kV to prevent knock-on damage of the graphene membranes.[39] With the C_s-value ($|C_s|$) set smaller than 5 μm, $\{1\bar{1}00\}$, lattice planes can be clearly revealed by HRTEM.

Conflict of Interest: The authors declare no competing financial interest.

Acknowledgment. We gratefully acknowledge support within the Cluster of Excellence "Engineering of Advanced Materials" (www.eam.uni-erlangen.de), the European Research Council (ERC; grant 246622-GRAPHENOCHEM) and the SFB 953 "Synthetic Carbon Allotropes" at the Friedrich-Alexander-Universität Erlangen-Nürnberg.

REFERENCES AND NOTES

1. Lee, C.; Wei, X.; Kysar, J. W.; Hone, J. Measurement of the Elastic Properties and Intrinsic Strength of Monolayer Graphene. *Science* **2008**, *321*, 385–388.
2. Bunch, J. S.; Verbridge, S. S.; Alden, J. S.; Van Der Zande, A. M.; Parpia, J. M.; Craighead, H. G.; McEuen, P. L. Impermeable Atomic Membranes from Graphene Sheets. *Nano Lett.* **2008**, *8*, 2458–2462.
3. Min, S. K.; Kim, W. Y.; Cho, Y.; Kim, K. S. Fast DNA Sequencing with a Graphene-Based Nanochannel Device. *Nat. Nanotechnol.* **2011**, *6*, 162–165.
4. Emtsev, K. V.; Bostwick, A.; Horn, K.; Jobst, J.; Kellogg, G. L.; Ley, L.; McChesney, J. L.; Ohta, T.; Reshanov, S. A.; Röhrl, J.; *et al.* Towards Wafer-Size Graphene Layers by Atmospheric Pressure Graphitization of Silicon Carbide. *Nat. Mater.* **2009**, *8*, 203–207.
5. Berger, C.; Song, Z.; Li, X.; Wu, X.; Brown, N.; Naud, C.; Mayou, D.; Li, T.; Hass, J.; Marchenkov, A. N.; *et al.* Electronic Confinement and Coherence in Patterned Epitaxial Graphene. *Science* **2006**, *312*, 1191–1196.
6. Lin, Y.-M.; Valdes-Garcia, A.; Han, S.-J.; Farmer, D. B.; Meric, I.; Sun, Y.; Wu, Y.; Dimitrakopoulos, C.; Grill, A.; Avouris, P.; *et al.* Wafer-Scale Graphene Integrated Circuit. *Science* **2011**, *332*, 1294–1297.
7. Hertel, S.; Waldmann, D.; Jobst, J.; Reshanov, S.; Schöner, A.; Krieger, M.; Weber, H. B. Tailoring the Graphene/Silicon Carbide Interface for Monolithic Wafer-Scale Electronics. *Nat. Commun.* **2012**, *3*, 957.
8. Tzalenchuk, A.; Lara-Avila, S.; Kalaboukhov, A.; Paolillo, S.; Syväjärvi, M.; Yakimova, R.; Kazakova, O.; Janssen, T. J. B. M.; Fal'ko, V. I.; Kubatkin, S. Towards a Quantum Resistance Standard Based on Epitaxial Graphene. *Nat. Nanotechnol.* **2010**, *5*, 186–189.
9. Novoselov, K. S.; Geim, A. K.; Morozov, S. V.; Jiang, D.; Zhang, Y.; Dubonos, S. V.; Grigorieva, I. V.; Firsov, A. A. Electric Field Effect in Atomically Thin Carbon Films. *Science* **2004**, *306*, 666–669.
10. Li, X.; Cai, W.; An, J.; Kim, S.; Nah, J.; Yang, D.; Piner, R.; Velamakanni, A.; Jung, I.; Tutuc, E.; *et al.* Large-Area Synthesis of High-Quality and Uniform Graphene Films on Copper Foils. *Science* **2009**, *324*, 1312–1314.
11. Park, S.; Ruoff, R. S. Chemical Methods for the Production of Graphenes. *Nat. Nanotechnol.* **2009**, *4*, 217–224.
12. Englert, J. M.; Dotzer, C.; Yang, G.; Schmid, M.; Papp, C.; Gottfried, J. M.; Steinr ü ck, H.-P.; Spiecker, E.; Hauke, F.; Hirsch, A. Covalent Bulk Functionalization of Graphene. *Nat. Chem.* **2011**, *3*, 279–286.
13. Meyer, J. C.; Kisielowski, C.; Erni, R.; Rossell, M. D.; Crommie, M. F.; Zettl, A. Direct Imaging of Lattice Atoms and Topological Defects in Graphene Membranes. *Nano Lett.* **2008**, *8*, 3582–3586.
14. Huang, P. Y.; Ruiz-Vargas, C. S.; van der Zande, A. M.; Whitney, W. S.; Levendorf, M. P.; Kevek, J. W.; Garg, S.; Alden, J. S.; Hustedt, C. J.; Zhu, Y.; *et al.* Grains and Grain Boundaries in Single-Layer Graphene Atomic Patchwork Quilts. *Nature* **2011**, *469*, 389–392.

15. Meyer, J. C.; Kurasch, S.; Park, H. J.; Skakalova, V.; Künzel, D.; Gross, A.; Chuvilin, A.; Algara-Siller, G.; Roth, S.; Iwasaki, T.; *et al.* Experimental Analysis of Charge Redistribution due to Chemical Bonding by High-Resolution Transmission Electron Microscopy. *Nat. Mater.* **2011**, *10*, 209–215.
16. Kim, K.; Lee, Z.; Regan, W.; Kisielowski, C.; Crommie, M. F.; Zettl, A. Grain Boundary Mapping in Polycrystalline Graphene. *ACS Nano* **2011**, *5*, 2142–2146.
17. Meyer, J. C.; Geim, A. K.; Katsnelson, M. I.; Novoselov, K. S.; Booth, T. J.; Roth, S. The Structure of Suspended Graphene Sheets. *Nature* **2007**, *446*, 60–63.
18. Suk, J. W.; Kitt, A.; Magnuson, C. W.; Hao, Y.; Ahmed, S.; An, J.; Swan, A. K.; Goldberg, B. B.; Ruoff, R. S. Transfer of CVD-Grown Monolayer Graphene onto Arbitrary Substrates. *ACS Nano* **2011**, *5*, 6916–6924.
19. Borysiuk, J.; Bożek, R.; Strupin′ski, W.; Baranowski, J. M. Graphene Growth on C and Si-Face of 4H-SiC—TEM and AFM Studies. *Mater. Sci. Forum* **2010**, *645−648*, 577–580.
20. Speck, F.; Jobst, J.; Fromm, F.; Ostler, M.; Waldmann, D.; Hundhausen, M.; Weber, H. B.; Seyller, T. The Quasi-Free-Standing Nature of Graphene on H-Saturated SiC-(0001). *Appl. Phys. Lett.* **2011**, *99*, 122106.
21. Emtsev, K. V.; Speck, F.; Seyller, T.; Ley, L. Interaction, Growth, and Ordering of Epitaxial Graphene on SiC{0001} Surfaces: A Comparative Photoelectron Spectroscopy Study. *Phys. Rev. B* **2008**, *77*, 155303.
22. Riedl, C.; Coletti, C.; Iwasaki, T.; Zakharov, A. A.; Starke, U. Quasi-Free-Standing Epitaxial Graphene on SiC Obtained by Hydrogen Intercalation. *Phys. Rev. Lett.* **2009**, *103*, 246804.
23. van Dorp, D. H.; Kelly, J. J. Photoelectrochemistry of 4H-SiC in KOH Solutions. *J. Electroanal. Chem.* **2007**, *599*, 260–266.
24. Shivaraman, S.; Barton, R. A.; Yu, X.; Alden, J.; Herman, L.; Chandrashekhar, M. V. S.; Park, J.; McEuen, P. L.; Parpia, J. M.; Craighead, H. G.; *et al.* Free-Standing Epitaxial Graphene. *Nano Lett.* **2009**, *9*, 3100–3105.
25. Cançado, L. G.; Jorio, A.; Ferreira, E. H. M.; Stavale, F.; Achete, C. A.; Capaz, R. B.; Moutinho, M. V. O.; Lombardo, A.; Kulmala, T.; Ferrari, A. C. Quantifying Defects in Graphene *via* Raman Spectroscopy at Different Excitation Energies. *Nano Lett.* **2011**, *11*, 3190–3196.
26. Lucchese, M. M.; Stavale, F.; Martins Ferreira, E. H.; Vilani, C.; Moutinho, M. V. O.; Capaz, R. B.; Achete, C. A.; Jorio, A. Quantifying Ion-Induced Defects and Raman Relaxation Length in Graphene. *Carbon* **2010**, *48*, 1592–1597.
27. Ferrari, A. C.; Meyer, J. C.; Scardaci, V.; Casiraghi, C.; Lazzeri, M.; Mauri, F.; Piscanec, S.; Jiang, D.; Novoselov, K. S.; Roth, S.; *et al.* Raman Spectrum of Graphene and Graphene Layers. *Phys. Rev. Lett.* **2006**, *97*, 187401.
28. Röhrl, J.; Hundhausen, M.; Emtsev, K. V.; Seyller, T.; Graupner, R.; Ley, L. Raman Spectra of Epitaxial Graphene on SiC(0001). *Appl. Phys. Lett.* **2008**, *92*, 201918.
29. Lee, D. S.; Riedl, C.; Krauss, B.; Von Klitzing, K.; Starke, U.; Smet, J. H. Raman Spectra of Epitaxial Graphene on SiC and of Epitaxial Graphene Transferred to SiO_2. *Nano Lett.* **2008**, *8*, 4320–4325.
30. Röhrl, J.; Hundhausen, M.; Speck, F.; Seyller, T. Strain and Charge in Epitaxial Graphene on Silicon Carbide Studied by Raman Spectroscopy. *Mater. Sci. Forum* **2010**, *645−648*, 603–606.
31. Graf, D.; Molitor, F.; Ensslin, K.; Stampfer, C.; Jungen, A.; Hierold, C.; Wirtz, L. Spatially Resolved Raman Spectroscopy of Single- and Few-Layer Graphene. *Nano Lett.* **2007**, *7*, 238–242.
32. Ferralis, N.; Maboudian, R.; Carraro, C. Evidence of Structural Strain in Epitaxial Graphene Layers on 6H-SiC(0001). *Phys. Rev. Lett.* **2008**, *101*, 156801.
33. Das, A.; Pisana, S.; Chakraborty, B.; Piscanec, S.; Saha, S. K.; Waghmare, U. V.; Novoselov, K. S.; Krishnamurthy, H. R.; Geim, A. K.; Ferrari, A. C.; *et al.* Monitoring Dopants by Raman Scattering in an Electrochemically Top-Gated Graphene Transistor. *Nat. Nanotechnol.* **2008**, *3*, 210–215.
34. Berciaud, S.; Ryu, S.; Brus, L. E.; Heinz, T. F. Probing the Intrinsic Properties of Exfoliated Graphene: Raman Spectroscopy of Free-Standing Monolayers. *Nano Lett.* **2009**, *9*, 346–352.
35. Reich, S.; Thomsen, C. Raman Spectroscopy of Graphite. *Philos. Trans. R. Soc., A* **2004**, *362*, 2271–2288.
36. Malard, L.; Elias, D.; Alves, E.; Pimenta, M. Observation of Distinct Electron-Phonon Couplings in Gated Bilayer Graphene. *Phys. Rev. Lett.* **2008**, *101*, 257401.
37. Mohiuddin, T.; Lombardo, A.; Nair, R.; Bonetti, A.; Savini, G.; Jalil, R.; Bonini, N.; Basko, D.; Galiotis, C.; Marzari, N.; *et al.* Uniaxial Strain in Graphene by Raman Spectroscopy: G Peak Splitting, Grüneisen Parameters, and Sample Orientation. *Phys. Rev. B* **2009**, *79*, 205433.
38. Carozo, V.; Almeida, C. M.; Ferreira, E. H. M.; Cançado, L. G.; Achete, C. A.; Jorio, A. Raman Signature of Graphene Superlattices. *Nano Lett.* **2011**, *11*, 4527–4534.
39. Meyer, J. C.; Eder, F.; Kurasch, S.; Skakalova, V.; Kotakoski, J.; Park, H. J.; Roth, S.; Chuvilin, A.; Eyhusen, S.; Benner, G.; *et al.* Accurate Measurement of Electron Beam Induced Displacement Cross Sections for Single-Layer Graphene. *Phys. Rev. Lett.* **2012**, *108*, 196102.